SCIENTIFIC REP⚙RTS

OPEN

Interface designed MoS₂/GaAs heterostructure solar cell with sandwich stacked hexagonal boron nitride

Shisheng Lin[1,2], Xiaoqiang Li[1], Peng Wang[1], Zhijuan Xu[1], Shengjiao Zhang[1], Huikai Zhong[1], Zhiqian Wu[1], Wenli Xu[1] & Hongsheng Chen[1,2]

MoS₂ is a layered two-dimensional semiconductor with a direct band gap of 1.8 eV. The MoS₂/bulk semiconductor system offers a new platform for solar cell device design. Different from the conventional bulk p-n junctions, in the MoS₂/bulk semiconductor heterostructure, static charge transfer shifts the Fermi level of MoS₂ toward that of bulk semiconductor, lowering the barrier height of the formed junction. Herein, we introduce hexagonal boron nitride (h-BN) into MoS₂/GaAs heterostructure to suppress the static charge transfer, and the obtained MoS₂/h-BN/GaAs solar cell exhibits an improved power conversion efficiency of 5.42%. More importantly, the sandwiched h-BN makes the Fermi level tuning of MoS₂ more effective. By employing chemical doping and electrical gating into the solar cell device, PCE of 9.03% is achieved, which is the highest among all the reported monolayer transition metal dichalcogenide based solar cells.

Two-dimensional (2D) materials provide rich physics in designing of new optoelectronic devices[1–4]. Because of the low light absorbance of the atomic thin 2D materials[5,6], the external semiconductor is usually incorporated to improve the performance of 2D material based devices[7–9]. Photodetectors based on monolayer graphene have been reported to show photo gain as high as ~10^8 and photo responsivity as high as ~10^7 A/W through the enhanced light absorption with covering semiconductor quantum dots on graphene[8]. Forming 2D materials/bulk materials heterostructure junctions is an alternative choice to obtain high performance optoelectronic devices as the bulk semiconductor can fully absorb incident light[10,11]. As the first discovered 2D material with many fascinating electrical and optical properties, graphene and its heterostructures have attracted much attention for solar cells worldwide[12–15]. Power conversion efficiency (PCE) of solar cells based on graphene/Si system has been improved from 1.65% to 15.6% since the first reported graphene/Si heterostructure solar cell in the year 2010[16,17]. Recently, we have reported graphene/GaAs solar cell with PCE of 18.5%[18]. On the other hand, single layer 2D molybdenum disulfide (MoS₂) is semiconductor with a direct band gap of 1.8 eV[19]. MoS₂ with thickness less than 1 nm can absorb 5–10% incident light[20]. Also, MoS₂ can be synthesized with large area by chemical vapor deposition (CVD) method[21–23]. Based on the abovementioned merits, the MoS₂/bulk semiconductor system offers a new platform for optoelectronic device design. It has been reported that MoS₂/Si heterostructure solar cell has an efficiency of 5.23% with the assistance of aluminum deposition on MoS₂[6]. However, much more work on MoS₂/semiconductor heterostructure is highly desirable both for the fundamental research interest and the potential photovoltaic application. Among all the bulk semiconductors, GaAs has a suitable direct band gap of 1.42 eV and high electron mobility (8000 cm²V⁻¹s⁻¹ at 300 K)[24], which makes itself one of the best candidates for high performance solar cells[25,26].

[1]Department of Information Science and Electronic Engineering, Zhejiang University, Hangzhou, 310027, China. [2]State Key Laboratory of Modern Optical Instrumentation, Zhejiang University, Hangzhou, 310027, China. Correspondence and requests for materials should be addressed to S.L. (email: shishenglin@zju.edu.cn) or H.C. (email: hansomchen@zju.edu.cn).
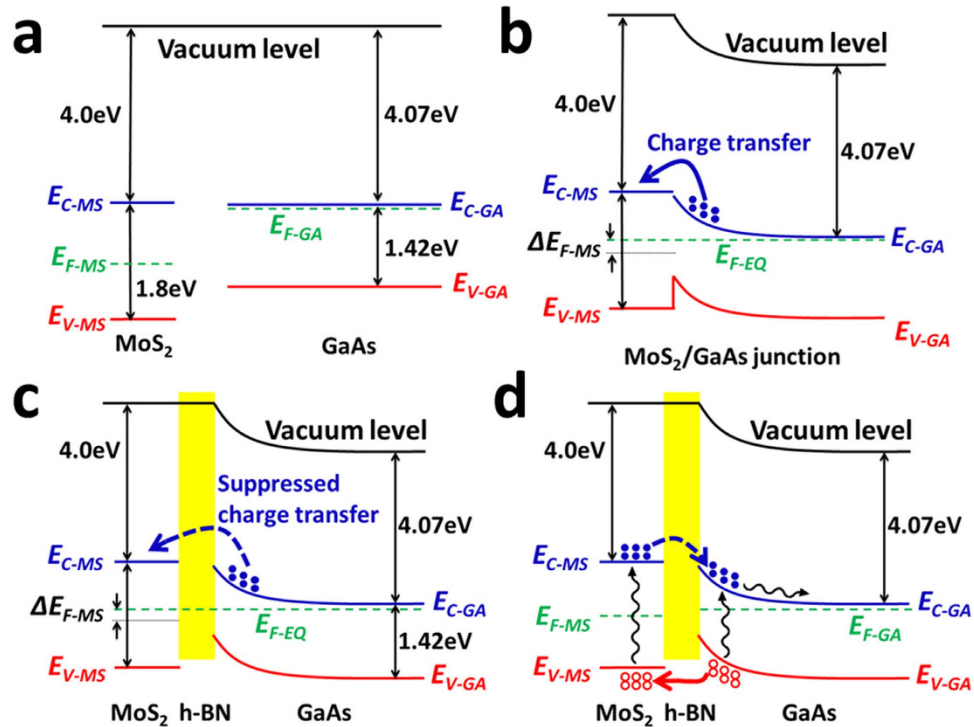
Figure 1. Schematic electronic band structure of independent MoS$_2$ and GaAs (**a**), MoS$_2$/GaAs Schottky junction (**b**), MoS$_2$/h-BN/GaAs heterojunction (**c**) under equilibrium condition and the electronic band structure of MoS$_2$/h-BN/GaAs heterojunction under illumination (**d**).

Tunable Fermi level is one of the unique physical properties of 2D materials, which can be finely tuned by chemical doping or electrical gating[27–30]. Different from the conventional bulk p-n junctions, there is static charge transfer between 2D materials and bulk semiconductor, which could severely lower the Fermi level difference between bulk semiconductor and 2D material[31], and lead to a decreased junction barrier height. The photovoltaic performance of the heterojunction is greatly influenced by the junction barrier height, which means suppressing the static charge transfer between 2D materials and semiconductor substrate are highly desirable. Herein, we introduce 2D hexagonal boron nitride (h-BN) into the MoS$_2$/GaAs heterostructure to suppress the static charge transfer. More importantly, the inserted h-BN layer makes the tuning of Fermi level of MoS$_2$ more effective, which greatly improves the performance of solar cells. Based on the interface band structure designing and Fermi level tuning of MoS$_2$, 9.03% of PCE has been achieved.

Results

Physical design of the MoS$_2$ based solar cell. The schematic electronic band structure of the independent MoS$_2$ and GaAs is shown in Fig. 1a. The electron affinity (energy gap between vacuum level and the bottom level of conduction band E$_{C-MS}$) of MoS$_2$ (χ_{MS}) is 4.0 eV[32], and the band gap of MoS$_2$ is 1.8 eV. As the measured sheet resistance of MoS$_2$ is in the range of 10^4–$10^6\,\Omega/\square$, indicating the Fermi level of MoS$_2$ (E$_{F-MS}$) locates near the middle of the band gap. The electron affinity of GaAs (χ_{GA}) is 4.07 eV. The Fermi level of GaAs (E$_{F-GA}$) used in this study locates around the bottom level of conduction band (E$_{C-GA}$) because the n-type doping concentration is around $10^{18}\,cm^{-3}$. When MoS$_2$ touches with GaAs, due to the Fermi level difference, some of majority electrons of GaAs inject into MoS$_2$, shifting E$_{F-MS}$ by ΔE$_{F-MS}$, as shown in Fig. 1b, which can be quantitatively expressed as:

$$\Delta E_{F-MS} = kTLn\left(\frac{\Delta n}{n_i}\right) \tag{1}$$

where Δn is the change of electron concentration in MoS$_2$ which affected by the injected electrons from GaAs, n_i is the intrinsic carrier concentration in MoS$_2$, k is the Boltzmann constant and T is the absolute temperature. The barrier height ($\Phi_{barrier}$) of the MoS$_2$/GaAs heterojunction can be presented as:

$$\Phi_{barrier} = \chi_{GA} - \chi_{MS} + (E_{F-GA} - E_{F-MS} - \Delta E_{F-MS}) \tag{2}$$
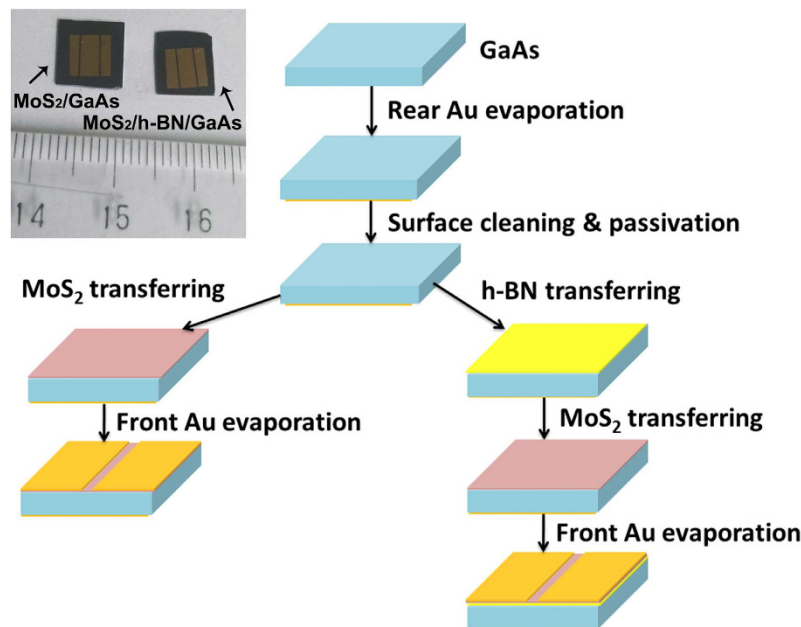
Figure 2. Schematic fabrication processes of MoS₂/GaAs and MoS₂/h-BN/GaAs Schottky junction based solar cells. The up-left inset shows the digital photographs of the corresponding devices. shows the digital photographs of the corresponding devices.

It is very clear that suppressing the static charge transfer during the formation of MoS₂/GaAs heterojunction can result in higher $\Phi_{barrier}$. We propose a device by inserting 2D h-BN into MoS₂/GaAs Schottky diode as the interface layer to suppress the static charge transfer. h-BN is one of 2D materials with a band gap of 5.9 eV and dielectric constant of 4.0[33]. The electronic band alignment of MoS₂/h-BN/GaAs heterojunction can be seen in Fig. 1c. As h-BN has a negative electron affinity[34], the electron transfer from GaAs to MoS₂ is suppressed during the formation of the MoS₂/h-BN/GaAs heterojunction. As a result, ΔE_{F-MS} is reduced and $\Phi_{barrier}$ of the junction is lifted up. Under illumination, photo generated excess electrons and holes are collected by GaAs and MoS₂, respectively. As shown in Fig. 1d, transport of holes from GaAs to MoS₂ is almost unaffected after inserting the ultrathin 2D BN layer, which dominates the power conversion from light to electricity. In other words, the open circuit voltage (V_{oc}) of the solar cell can be increased by the inserted h-BN while short circuit current density (J_{sc}) stays almost unchanged, thus, solar cell with a better performance can be expected.

Fig. 2 shows the schematic fabrication processes of MoS₂/GaAs and MoS₂/h-BN/GaAs Schottky junction based solar cells. After removal of the native oxide on the GaAs substrate, Au with a thickness of 60 nm was evaporated on the rear surface of GaAs forming ohmic contact. Then the front surface of GaAs was cleaned with dilute HCl aqueous solution. Front surface passivation is achieved with remote NH₃ plasma treatment for 5 min with power of 120 Watt and frequency of 27.5 MHz. After the passivation treatment, h-BN and MoS₂ in sequence or MoS₂ alone is directly transferred onto the front surface of GaAs substrate, followed with the deposition of front Au contacts (60 nm) with mask. Inset in Fig. 2 shows the digital photographs of the typical MoS₂/GaAs and MoS₂/h-BN/GaAs heterojunction based solar cells, where the thin line shape of the active area can be seen, which is designed for efficiently current collection based on the high resistance of monolayer MoS₂.

Basic properties of the MoS₂/h-BN/GaAs heterostructure solar cell. Fig. 3a shows the schematic cross section structure of the MoS₂/h-BN/GaAs heterojunction solar cell, which is composed of rear Au contact, GaAs substrate, h-BN layer, MoS₂ layer and the front Au contact from bottom to top. The active area of the device is defined with the opened window in the front Au contact, as shown in Fig. 3b. The width of the active area is 120 μm and the length is 5 mm, making the active area 0.6 mm². As the thickness of the front Au contact is 60 nm, no light can be absorbed by the device in the Au shadowed area, which guarantees the precise active area. The high resolution transmission electron microscopy (HRTEM) image of the MoS₂ is shown in Fig. 3c, which shows the six fold symmetry nature of the MoS₂. The inset of the Fig. 3c shows the HRTEM image of MoS₂ layer, which clearly indicates the CVD grown MoS₂ is monolayer. The electron diffraction pattern can be seen in Supplementary Information Fig. S1, which also implies the monolayer nature of MoS₂. Fig. 3d shows the absorption spectrum of the CVD grown MoS₂, where three absorption peaks corresponding to 436 nm, 619 nm and 662 nm can be seen in the wavelength range of 350–800 nm. The peak of the absorbance locates at 436 nm is 8.9%, which is in agreement with the reported absorbance of the monolayer MoS₂[20]. The Raman spectrum of the
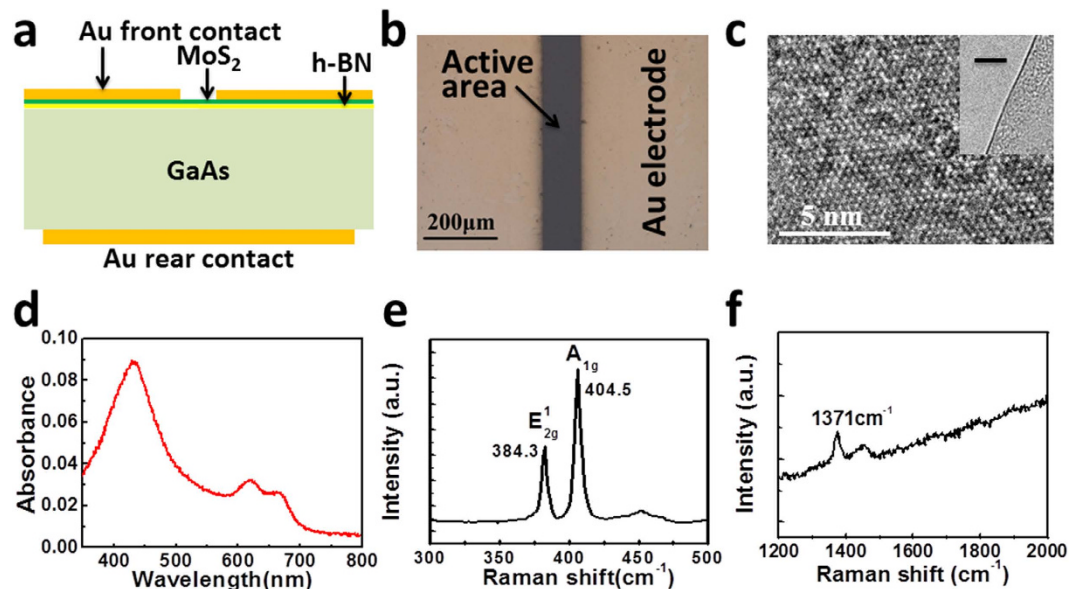
Figure 3. (**a**) Schematic structure of the MoS$_2$/h-BN/GaAs heterostructure. (**b**) Optical micrograph of the MoS$_2$/h-BN/GaAs solar cell. (**c**) HRTEM of the monolayer MoS2, inset is the TEM image of the edge of the MoS$_2$ layer, where the bar represents 10 nm. (**d**) Absorption spectrum of the monolayer MoS$_2$. Raman spectra of monolayer MoS$_2$ (**e**) and monolayer h-BN (**f**) used in this study.

MoS$_2$ on Si/SiO$_2$ substrate is shown in Fig. 3e. The Raman peaks corresponding to E$^1_{2g}$ and A$_{1g}$ modes of MoS$_2$ locate at 384.3 cm^{-1} and 404.5 cm^{-1}, respectively, indicating the grown MoS$_2$ is monolayer[35]. Fig. 3f presents the Raman spectrum of h-BN, where the 1371 cm^{-1} peak indicates it is monolayer[36]. The digital photographs of transferred h-BN on Si/SiO$_2$ substrate, optical microscopy image and atomic force microscopy image of MoS$_2$ and optical microscopy image of h-BN can be seen in Supplementary Information Fig. S2, where can be seen that the homogeneity of CVD grown MoS$_2$ and h-BN is good.

Fig. 4a shows the dark current density-voltage (*J-V*) curves of the MoS$_2$/GaAs and MoS$_2$/h-BN/GaAs heterojunctions, both of which show good rectifying characteristics. It is noteworthy that in this study if no mentioned, GaAs substrate is n-type doped. We also test the *J-V* curve of MoS$_2$/p-GaAs, which shows bad rectifying characteristics as presented in Supplementary Information Figure S3. The threshold voltage (the voltage needed to reach a current density of 2 mA/cm^2 here) for the MoS$_2$/GaAs heterojunction is 0.41 V, while the value for the MoS$_2$/h-BN/GaAs hetrostructure is 0.52 V, suggesting that $\Phi_{barrier}$ is increased by the interlayer h-BN. The value of $\Phi_{barrier}$ can be deduced through fitting of dark *J-V* curves as expressed by:

$$J = J_0 (\exp \frac{qV}{N_{IF}KT} - 1) \tag{3}$$

where *K* is the Boltzmann constant, N_{IF} is the junction ideality factor and *q* is the value of electron charge. Based on thermionic-emission theory, saturation current density J_0 can be described as:

$$J_0 = A^* T^2 \exp\left(-\frac{q\Phi_{barrier}}{KT}\right) \tag{4}$$

where A^* is the effective Richardson's constant of n-type GaAs (8.16 A/k•cm^2)[37]. Based on equations (3) and (4), the values of N_{IF} for MoS$_2$/GaAs and MoS$_2$/h-BN/GaAs heterojunctions are 3.18 and 2.73, and the $\Phi_{barrier}$ values are 0.71 eV and 0.78 eV, respectively. The lower N_{IF} of the MoS$_2$/h-BN/GaAs device compared with that of the MoS$_2$/GaAs device indicates that the interface recombination rate is decreased with interlayer h-BN. Fig. 4b shows the *J-V* curves of the MoS$_2$/GaAs and MoS$_2$/h-BN/GaAs heterostructure solar cell under AM1.5G illumination. As $\Phi_{barrier}$ is increased, with interlayer h-BN, V_{oc} of the solar cell is increased from 0.51 V to 0.57 V, while the J_{sc} is slightly decreased from 20.6 mA/cm^2 to 20.2 mA/cm^2. With the values of fill factor (FF, FF = P$_{max}$/(V$_{oc}$ × J$_{sc}$)) as 45.9% and 47.0%, the PCE values (PCE = V$_{oc}$ × J$_{sc}$ × FF) for the MoS$_2$/GaAs and MoS$_2$/h-BN/GaAs solar cells are 4.82% and 5.42%, respectively. The series resistance (R_s) fitting results of the MoS$_2$/GaAs and MoS$_2$/h-BN/GaAs solar cells are shown in Fig. 4c, which demonstrates R_s is increased from 56.8 Ω for the MoS$_2$/GaAs device to the value of 81.9 Ω for the MoS$_2$/h-BN/GaAs device. FF is mainly influenced by N_{IF} and R_s. Lower N_{IF} leads
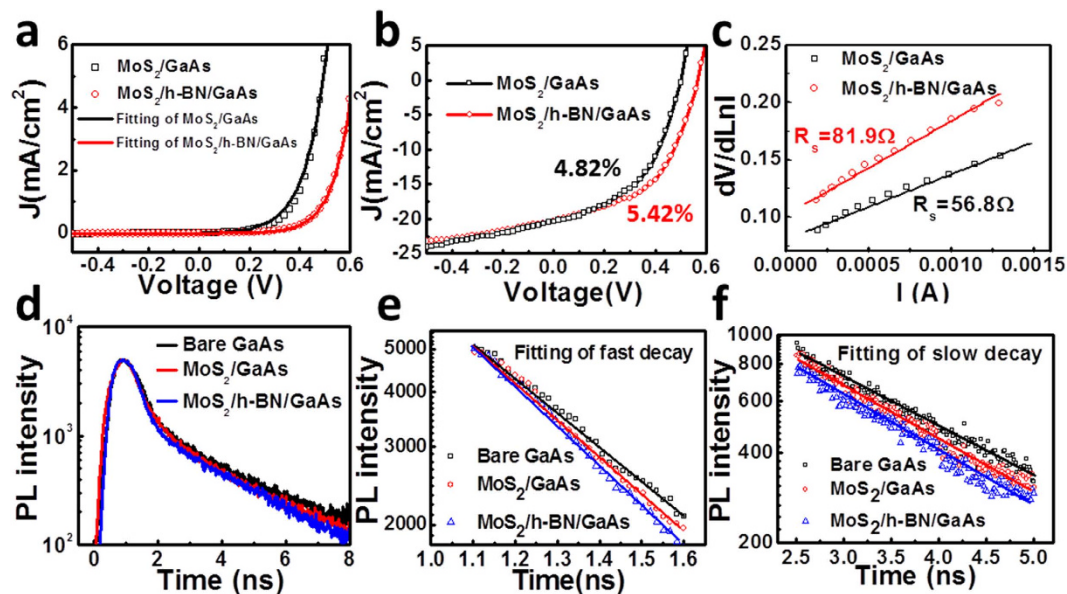
Figure 4. (**a**) Dark J-V curves of the MoS$_2$/GaAs and MoS$_2$/h-BN/GaAs heterojunctions. (**b**) J-V curves of the MoS$_2$/GaAs and MoS$_2$/h-BN/GaAs heterojunctions under AM1.5G illumination. (**c**) Linear fitting of dV/dLnI~I data for obtaining R$_s$ of the devices. (**d**) Transient PL of the bare GaAs substrate, MoS$_2$/GaAs and MoS$_2$/h-BN/GaAs heterojunctions. (**e**) Fitting of the PL decay time constant in the fast decay range and (**f**) in the slow decay range.

to higher FF while higher R_s leads to lower FF. For the MoS$_2$/h-BN/GaAs device, even with increased R_s, the decreased N_{IF} increases the FF compared with the value of MoS$_2$/GaAs device.

The electrical properties mentioned above indicate the importance of the interface recombination condition for the MoS$_2$/GaAs and MoS$_2$/h-BN/GaAs devices. Here transient photoluminescence (PL) is employed to investigate the kinetics of the photo generated carriers near the interface. Fig. 4d shows the transient PL decay curves for bare GaAs substrate, and the same MoS$_2$/GaAs and MoS$_2$/h-BN/GaAs heterostructure devices with PCE of 4.82% and 5.42% respectively. The decay curves show double channel dependent behavior, corresponding to a fast decay channel (in the range of 1 ns to 2 ns) and a slow decay channel (after 2 ns). The wavelength of the excitation laser is 450 nm, and the absorption depth is close to the surface of GaAs (about 50 nm). The quick decay range in the first nanosecond is related to carrier kinetics at surface or interface, and the subsequent slow decay range is dominated by the bulk recombination processes. PL decay time constants are deduced by exponentially fitting the PL intensity decay curves in the fast and slow decay ranges as shown in Fig. 4e,f, respectively. The fitted PL decay time constants in the fast decay range for bare GaAs, MoS$_2$/GaAs and MoS$_2$/h-BN/GaAs are 0.97 ns, 0.59 ns and 0.52 ns, respectively, and the values in the slow decay range are 1.92 ns, 1.89 ns and 1.85 ns, respectively. For the bare GaAs, photo generated excess carriers recombine with emission of photons or phonons. In MoS$_2$/GaAs heterostructure, besides the process mentioned above, parts of the excited holes in GaAs are separated by the heterojunction and collected by MoS$_2$. The separated electrons and holes cannot participate in the radiation recombination process. Thus PL decay time constant is decreased. In the MoS$_2$/h-BN/GaAs heterostructure, $\Phi_{barrier}$ is increased, which leads to higher speed of carrier separation process and even shorter PL decay time constant. Recombination will take place when electrons produced in GaAs cross the interface. The recombination rate is influenced by the carriers crossing time, which corresponds to the PL decay time constant in the fast decay range. For the device with interlayer h-BN, crossing time is shortened, resulting in the lowered interface recombination rate and lower value of N_{IF}. For the PL decay in the slow decay range, similar time constants imply that the PL decay process is dominated by the bulk recombination properties.

Enhance the performance of the MoS$_2$/h-BN/GaAs heterostructure solar cell by chemical doping. The Fermi level and carrier concentration in MoS$_2$ can be tuned by chemical doping. In this study, AuCl$_3$ solution in nitromethane (1 mM) is used to doping 2D MoS$_2$ to increase the PCE of the MoS$_2$/h-BN/GaAs solar cell. The J-V curves in the dark and under AM1.5G illumination can be found in Fig. 5a. The threshold voltage increases from 0.45 V to 0.58 V for after doping of MoS$_2$, indicating $\Phi_{barrier}$ increases by AuCl$_3$ doping of MoS$_2$. The value of $\Phi_{barrier}$ can be deduced through fitting of dark J-V curves based on equation (3) and (4). The obtained values are 0.79 eV and 0.85 eV for the undoped and doped MoS$_2$/h-BN/GaAs devices, respectively. As $\Phi_{barrier}$ increases, V_{oc} of the MoS$_2$/h-BN/GaAs heterostructure based solar cell increases from 0.56 V to 0.64 V. Meanwhile, J_{sc} is slightly increased from 20.6 mA/cm^2
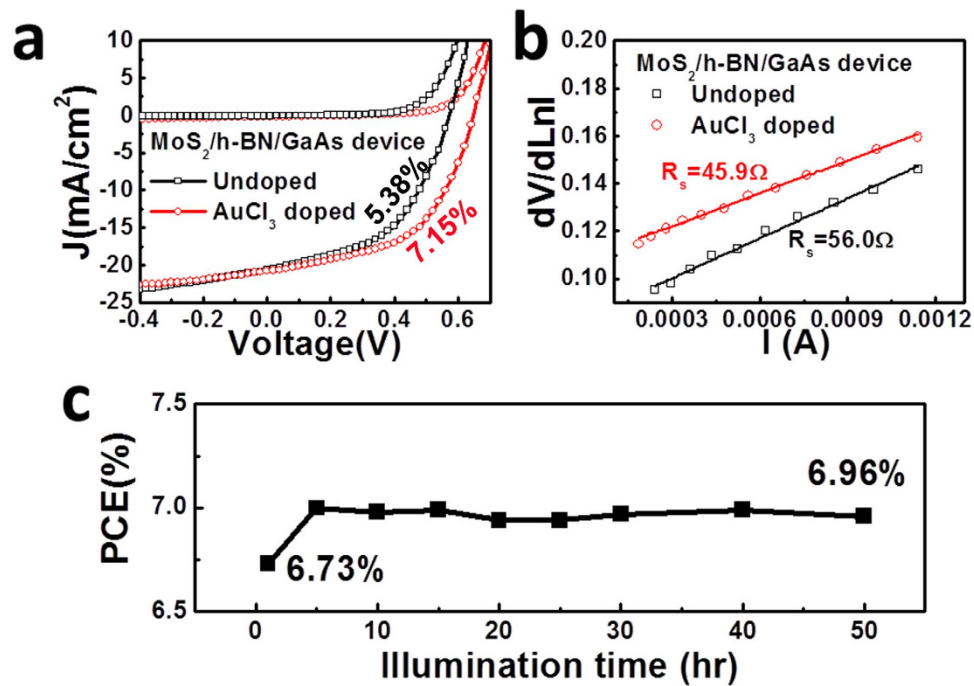
Figure 5. (**a**) *J-V* curves in the dark and under AM1.5G illumination of undoped and doped MoS$_2$/h-BN/GaAs solar cells. (**b**) R_s fitting of the MoS$_2$/h-BN/GaAs solar cell device with and without AuCl$_3$ doping. (**c**) Performance stability of the MoS$_2$/h-BN/GaAs solar cell under AM1.5G illumination.

to 20.8 mA/cm^2. The FF values are 46.6% and 53.7%, and the PCE values are 5.38% and 7.15% for the undoped and doped devices, respectively. The increase of the FF after doping is related to the decrease of R_s, as shown in Fig. 5b, the value of R_s without doping of MoS$_2$ is 56.0 Ω, while R_s is decreased to 45.9 Ω after doping. In addition, to explore the stability of the doped MoS$_2$/h-BN/GaAs solar cell, we test the variation of the PCE values in 50 hours under AM1.5G illumination, as seen in Fig. 5c. The device was sealed by polymethyl methacrylate (PMMA) through spining-on-coating. The starting PCE value is 6.73%, while after illumination for 50 hrs, the PCE increases to 6.96%. Considering the light induced degradation of crystaslline silicon solar cell is usually happened in the first 24 hrs under AM1.5G illumination, it can be safely concluded the stability of MoS$_2$/h-BN/GaAs solar cell under illumination is good with suitable encapsulation.

Further improvement of the MoS$_2$/h-BN/GaAs heterostructure solar cell by electrical gating.
As a atomic thin 2D semoconductor, the Fermi level of MoS$_2$ can be finely tuned with gating effect[38]. Here we employ PEO based ion polymer as the top gate electrode[39], and the schematic structure of the field effect MoS$_2$/h-BN/GaAs solar cell is shown in Fig. 6a. Ion gate is directly covered on the surface of AuCl$_3$ doped MoS$_2$. Negative voltage is applied on the ion gate and the rear Au contact is connected to the ground. Fig. 6b shows the *J-V* curves of the field effect solar cell under AM1.5G illumination. When gate voltage (V_{gate}) equals to -0.5 V, V_{oc} of the solar cell is increased from 0.64 V to 0.72 V. Meanwhile, J_{sc} is slightly increased from 20.2 mA/cm^2 to 20.7 mA/cm^2, which might be attributed to the enhanced efficiency of charge seperation with gating. FF is increased from 53.1% to 54.9% and PCE is improved from 6.87% to 8.27%. when V_{gate} equals to -1.0 V, the obtained values of V_{oc}, J_{sc} and FF are 0.76 V, 21.1 mA/cm^2 and 56.3%, respectively. And the final PCE is 9.03%. Fig. 6c shows the dark *J-V* curves with different V_{gate}. The threshold voltage is increased when the negative V_{gate} increases. By fitting of the dark *J-V* curves shown in Fig. 6c, values of $\Phi_{barrier}$ can be obtained and shown in Fig. 6d, where the values of V_{oc} corresponding to different V_{gate} are also shown. Fig. 6d discloses that the increased V_{oc} is mainly attributed to the improved $\Phi_{barrier}$ under gating effect. The $\Phi_{barrier}$ values are 0.85 eV, 0.91 eV and 0.95 eV corresponding to the V_{gate} values of 0 V, -0.5 V and -1.0 V, respectively. V_{gate} higher than -1.0 V causes gate leakage current in this experiment, causing the dark *J-V* curves away from the (0, 0) point and the *J-V* curves under illumination unreliable. Thus no further *J-V* curves are shown here for V_{gate} higher than -1.0 V. The effect of electrical gating on the MoS$_2$/GaAs solar cell is shown in Supplementary Information Fig. S4. The PCE values are 4.71%, 5.81% and 6.15% with the Voc values as 0.50 V, 0.55 V and 0.57 V corresponding to the V_{gate} values of 0 V, -0.5 V and -1.0 V, respectively. The $\Phi_{barrier}$ values correspondingly are 0.67 eV, 0.71 eV and 0.74 eV. The change of $\Phi_{barrier}$ is 0.07 eV, suggesting the Fermi level of MoS$_2$ is shifted by 0.07 eV with the gate voltage of -1.0 V. For the MoS$_2$/h-BN/GaAs device, Fermi level of MoS$_2$ can be tuned by 0.10 eV as $\Phi_{barrier}$ is increased by 0.10 eV, 43% higher than that of
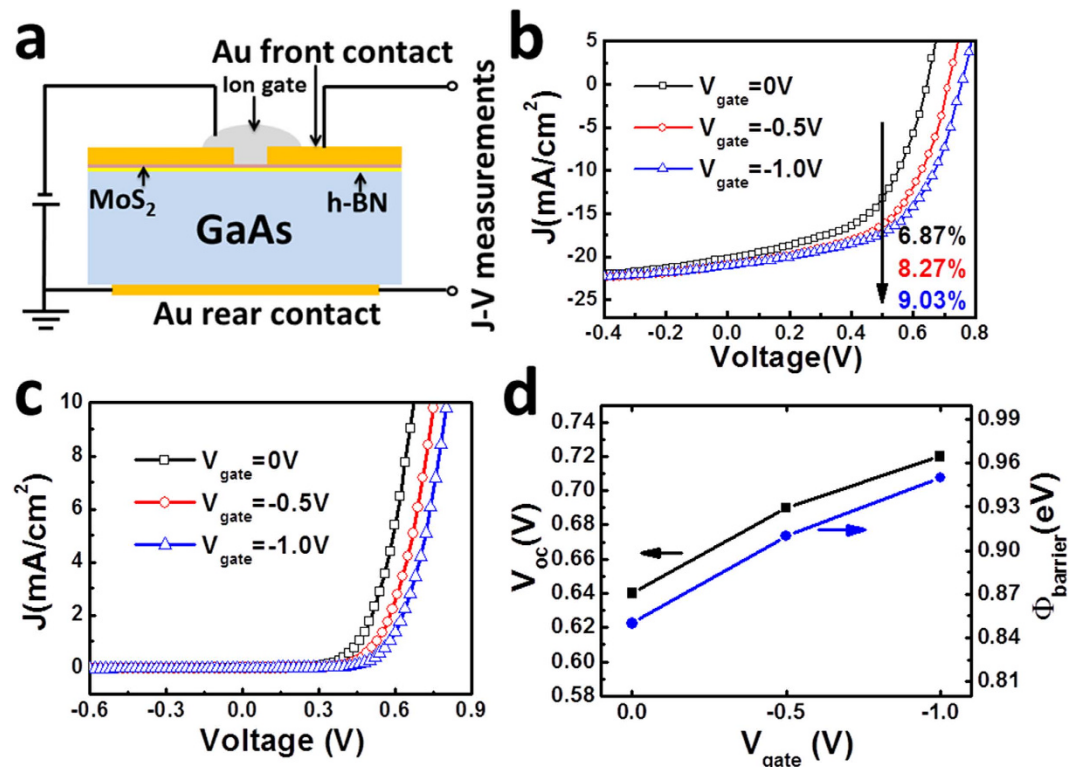
Figure 6. (**a**) Schematic structure of the field effect MoS$_2$/h-BN/GaAs solar cell. (**b**) J-V curves of the field effect MoS$_2$/h-BN/GaAs heterojunctions under AM1.5G illumination and different V_{gate}. (**c**) Dark J-V curves of the field effect MoS$_2$/h-BN/GaAs heterojunctions under different V_{gate}. (**d**) Values of $\Phi_{barrier}$ and V_{oc} correspond to different V_{gate}.

the MoS$_2$/GaAs device. In the 2D material/semiconductor heterostructure, change of the Fermi level of the 2D material can be suppressed by the charge transfer from GaAs substrate. In the MoS$_2$/GaAs device, downshifting the Fermi level of MoS$_2$ is inhibited by the electron transfer from GaAs to MoS$_2$. By intersting h-BN to suppress the electron transfer, Fermi level tuning of MoS$_2$ by the electrical gating can be more effective. From this point of view, interface h-BN can not only increase the initial $\Phi_{barrier}$ of the MoS$_2$/h-BN/GaAs heterostructure, but also guarantees more effectively Fermi level tuning of MoS$_2$.

Discussion

MoS$_2$/GaAs heterostructure based solar cell is investigated. Different from the traditional p-n junctions and metal/semiconductor Schottky junctions, the charge transfer between MoS$_2$ and the GaAs substrate can greatly influence the position of Fermi level in the 2D material, which leads to a much lower barrier height than the ideal value originated from the Fermi level difference. The barrier height is a key factor for the electrical properties of electronic and optoelectronic devices. Thus, suppressing or preventing the charge transfer during the formation of the 2D material based heterojunctions is highly desired to achieve high performance devices. Herein, we demonstrated the performance of MoS$_2$/GaAs based heterostructure solar cell is improved by inserting interlayer h-BN. The inserted h-BN layer can suppress the electron injection from n-type GaAs into MoS$_2$ during the junction formation, while does not affect the hole separation and collection processes according to the electronic band structure of h-BN. Thus, PCE is increased from 4.82% to 5.42% after inserting the BN layer as higher barrier height and V$_{oc}$ can be achieved. Furthermore, by employing chemical doping and electrical gating into the solar cell device, PCE of 9.03% is achieved, which is the highest among all the reported monolayer transition-metal dichalcogenide-based solar cells. This physical picture and technique could be extended into other 2D materials/semiconductor heterostructure based electronic and optoelectronic devices.

Methods

Monolayer h-BN was grown on copper substrate with B$_3$N$_3$H$_6$ as the precursor at 1000 °C for 30 min[40]. Single layer MoS$_2$ film was grown on Si/SiO$_2$ substrate in a quartz tube with CVD method[41]. MoO$_3$ powder and sulfur powder (99.9%, both bought from Aladdin) was used as the precursor. Growth temperature was set at 650 °C. 60 nm Au was thermally evaporated on back surface of GaAs to form rear contact. GaAs substrate was cleaned by dipping the samples into 10%wt HCl solution for 5 min followed with DI water rinse. Surface passivation of GaAs was realized by remote NH$_3$ plasma treatment for 5 min

with 120 Watt 27.5 MHz RF generator. h-BN was transferred onto the GaAs substrate using PMMA as the sacrificing layer. After PMMA spun-on, MoS$_2$ on Si/SiO$_2$ substrate was immersed into deionized water to lift-off the PMMA-MoS$_2$ films. After transferring, PMMA was removed by immersing the samples into acetone for 20 min.

MoS$_2$ and h-BN were characterized by Raman spectroscopy (Renishaw inVia Reflex) with the excitation wavelength of 532 nm. The microstructure of MoS$_2$ was examined by HRTEM (Tecnai F-20 operating at 200 KV). Atomic force Microscopy (AFM) characterization was performed using Veeco dimension 3100 system. The MoS$_2$/h-BN/GaAs solar devices were tested by Agilent B1500A system with a solar simulator under AM1.5G condition. It is noteworthy that the illumination intensity was calibrated with a standard Si solar cell. Transient PL measurements were used to evaluate the charge recombination and separation behaviors at the interfaces of MoS$_2$/h-BN/GaAs heterojunction. The excitation light source (PicoHarp 300 system) was a 450 nm pulsed laser with 1 MHz repetition rate and 50 ps pulse duration with power of 10 μW. The diameter of the excitation laser spot was 10 μm. The PL signal with wavelength shorter than 1100 nm was collected by a multimode optical fiber and recorded by a Horiba Jobin Yvon iHR550 spectrometer. All spectra were collected until the peak value reaching 5000 counts.

References

1. Geim, A. K. & Novoselov, K. S. The rise of graphene. *Nat. Mater.* **6,** 183–191 (2007).
2. Geim, A. K. Graphene: Status and prospects. *Science* **324,** 1530–1534 (2009).
3. Geim, A. K. & Grigorieva, I. V. Van der Waals heterostructures. *Nature* **499,** 419–425 (2013).
4. Novoselov, K. S. *et al.* Two-dimensional gas of massless Dirac fermions in graphene. *Nature* **438,** 197–200 (2005).
5. Nair, R. R. *et al.* Fine structure constant defines visual transparency of graphene. *Science* **320,** 1308–1308 (2008).
6. Tsai, M. L. *et al.* Monolayer MoS$_2$ heterojunction solar cells. *ACS Nano* **8,** 8317–8322 (2014).
7. Gan, X. T. *et al.* Chip-integrated ultrafast graphene photodetector with high responsivity. *Nat. Photonics* **7,** 883–887 (2013).
8. Konstantatos, G. *et al.* Hybrid graphene-quantum dot phototransistors with ultrahigh gain. *Nat. Nanotechnol.* **7,** 363–368 (2012).
9. Zhang, W. J. *et al.* Ultrahigh-gain photodetectors based on atomically thin graphene-MoS$_2$ heterostructures. *Sci. Rep.* **4,** 03826 (2014).
10. Zeng, L. H. *et al.* Monolayer graphene/germanium Schottky junction as high-performance self-driven infrared light photodetector. *ACS Appl. Mater. Inter.* **5,** 9362–9366 (2013).
11. Wang, X. J. *et al.* Photo-induced doping in graphene/silicon heterostructures. *J. Phys. Chem. C* **119,** 1061–1066 (2015).
12. Miao, X. C. *et al.* High efficiency graphene solar cells by chemical doping. *Nano Lett.* **12,** 2745–2750 (2012).
13. Shi, E. Z. *et al.* Colloidal antireflection coating improves graphene-silicon solar cells. *Nano Lett.* **13,** 1776–1781 (2013).
14. Zhang, X. Z. *et al.* High-efficiency graphene/Si nanoarray Schottky junction solar cells via surface modification and graphene doping. *J. Mater. Chem. A* **1,** 6593–6601 (2013).
15. Brus, V. V. *et al.* Stability of graphene-silicon heterostructure solar cells. *Phys. Status Solidi A* **211,** 843–847 (2014).
16. Li, X. M. *et al.* Graphene-on-silicon Schottky junction solar cells. *Adv. Mater* **22,** 2743–2748 (2010).
17. Song, Y. *et al.* Role of interfacial oxide in high-efficiency graphene-silicon Schottky barrier solar cells. *Nano Lett.* **15,** 2104–2110 (2015).
18. Li, X. Q. *et al.* 18.5% efficient graphene/GaAs van der Waals heterostructure solar cell. *Nano Energy*, doi: 10.1016/j.nanoen.2015.07.003 (2015).
19. Lei, T. M. *et al.* Electronic structure and optical properties of monolayer MoS$_2$. *Rare Metal Mat. Eng.* **42,** 2477–2480 (2013).
20. Bernardi, M., Palummo, M. & Grossman, J. C. Extraordinary sunlight absorption and one nanometer thick photovoltaics using two-dimensional monolayer materials. *Nano Lett.* **13,** 3664–3670 (2013).
21. Li, B. *et al.* Growth of large area few-layer or monolayer MoS$_2$ from controllable MoO$_3$ nanowire nuclei. *RSC Adv.* **4,** 26407–26412 (2014).
22. McCreary, K. M. *et al.* Large-area synthesis of continuous and uniform MoS$_2$ monolayer films on graphene. *Adv. Funct. Mater.* **24,** 6449–6454 (2014).
23. Lan, F. F. *et al.* Epitaxial growth of single-crystalline monolayer MoS$_2$ by two-step method. *ECS Solid State Lett.* **4,** 19–21 (2015).
24. Vorobev, V. N. & Sokolov, Y. F. Determination of mobility in small samples of gallium arsenide from magnetoresistive effects. *Sov. Phys. Semicond.* **5,** 616–620 (1971).
25. Bauhuis, G. J., Mulder, P., Haverkamp, E. J., Huijben, J. C. C. M. & Schermer, J. J. 26.1% thin-film GaAs solar cell using epitaxial lift-off. *Sol. Energ. Mat. Sol. C* **93,** 1488–1491 (2009).
26. Belghachi, A., Helmaoui, A. & Cheknane, A. High efficiency all-GaAs solar cell. *Prog. Photovoltaics* **18,** 79–82 (2010).
27. Das, A. *et al.* Monitoring dopants by Raman scattering in an electrochemically top-gated graphene transistor. *Nat. Nanotechnol.* **3,** 210–215 (2008).
28. Chen, C. C., Chang, C. C., Li, Z., Levi, A. F. J. & Cronin, S. B. Gate tunable graphene-silicon Ohmic/Schottky contacts. *Appl. Phys. Lett.* **101,** 223113 (2012).
29. Xu, H. *et al.* High responsivity and gate tunable graphene-MoS$_2$ hybrid phototransistor. *Small* **10,** 2300–2306 (2014).
30. Kummell, T., Quitsch, W., Matthis, S., Litwin, T. & Bacher, G. Gate control of carrier distribution in k-space in MoS$_2$ monolayer and bilayer crystals. *Phys. Rev. B* **91,** 125305 (2015).
31. Zhong, H. J. *et al.* Charge transport mechanisms of graphene/semiconductor Schottky barriers: A theoretical and experimental study. *J. Appl. Phys.* **115,** 013701 (2014).
32. Li, H.-M. *et al.* Metal-semiconductor barrier modulation for high photoresponse in transition metal dichalcogenide field effect transistors. *Sci. Rep.* **4,** 04041 (2014).
33. Kim, K. K. *et al.* Synthesis and characterization of hexagonal boron nitride film as a dielectric layer for graphene devices. *ACS Nano* **6,** 8583–8590 (2012).
34. Powers, M. J. *et al.* Observation of a negative electron affinity for boron nitride. *Appl. Phys. Lett.* **67,** 3912–3914 (1995).
35. Li, H. *et al.* From bulk to monolayer MoS$_2$: evolution of Raman scattering. *Adv. Funct. Mater.* **22,** 1385–1390 (2012).
36. Gorbachev, R. V. *et al.* Hunting for monolayer boron nitride: Optical and Raman signatures. *Small* **7,** 465–468 (2011).
37. Carpenter, M. S., Melloch, M. R. & Dungan, T. E. Schottky-barrier formation on (NH$_4$)$_2$S-treated n-type and p-type (100) GaAs. *Appl. Phys. Lett.* **53,** 66–68 (1988).
38. Wang, W. Y. *et al.* Controllable Schottky barriers between MoS$_2$ and permalloy. *Sci. Rep.* **4,** 06928 (2014).
39. Chen, C. C., Chang, C. C., Li, Z., Levi, A. F. J. & Cronin, S. B. Gate tunable graphene-silicon Ohmic/Schottky contacts. *Appl. Phys. Lett.* **101,** 223113 (2012).

40. Kim, K. K. *et al.* Synthesis of monolayer hexagonal boron nitride on Cu foil using chemical vapor deposition. *Nano Lett.* **12,** 161–166 (2012).
41. Y. H. Lee *et al.* Synthesis of large-area MoS$_2$ atomic layers with chemical vapor deposition. *Adv. Mater.* **24,** 2320–2325 (2012).

Author Contributions

S.S. Lin initiated this work. X.Q.L., S.S.L., P.W., S.J.Z., Z.J.X., H.K.Z., Z.Q.W. and W.L.X. performed the experiments. X.Q.L., S.S.L. and H.S.C. analyzed the data. S.S.L., X.Q.L. and H.S.C. write the paper and all authors comment on this paper.

Additional Information

Supplementary information accompanies this paper at http://www.nature.com/srep

Competing financial interests: The authors declare no competing financial interests.

How to cite this article: Lin, S. *et al.* Interface designed MoS$_2$/GaAs heterostructure solar cell with sandwich stacked hexagonal boron nitride. *Sci. Rep.* **5**, 15103; doi: 10.1038/srep15103 (2015).